Fermi National Accelerator Laboratory

FSU-HEP-910621
FERMILAB-PUB-91/163-T
June 1991

AN ORDER α_s CALCULATION OF HADRONIC $W^{\pm}Z$ PRODUCTION

J. OHNEMUS

*Department of Physics**
Florida State University
Tallahassee, Florida 32306

and

Fermi National Accelerator Laboratory
P.O. Box 500, Batavia, IL 60510

ABSTRACT

An order α_s calculation of $p\overset{(-)}{p} \to W^{\pm}Z + X$ is presented. Results are given for the total cross section and differential distributions for Tevatron, LHC, and SSC energies. The calculation utilizes a combination of analytic and Monte Carlo integration methods which makes it easy to calculate a variety of observables and to impose experimental cuts.

---

* *Permanent address*

Operated by Universities Research Association Inc. under contract with the United States Department of Energy

1. INTRODUCTION

The production of $W^{\pm}Z$ pairs at hadron supercolliders will be an important process for testing the standard model.[1] The observation of $W^{\pm}Z$ pairs provides a test of two crucial parts of the standard model that lack experimental verification, namely, the gauge-boson self-interactions and the electroweak symmetry breaking mechanism. In order to perform these tests it is important to have precise calculations of $W^{\pm}Z$ production to compare with the experimental measurements.

In the standard model the $W^{\pm}$, Z, and γ are the gauge bosons of a local SU(2)×U(1) symmetry which governs the interactions between the gauge bosons. There are important cancellations in the standard model amplitudes for $W^{\pm}Z$ production which rely on the gauge structure of the WWZ trilinear coupling. Anomalous couplings at the WWZ vertex will lead to enhancements in the $W^{\pm}Z$ cross section at high invariant masses.[2]

The $W^{\pm}$ and Z bosons acquire masses due to the spontaneous breakdown of the SU(2)×U(1) symmetry. Although the mechanism responsible for spontaneous symmetry breaking is unknown, there are two possibilities: either there is a scalar particle much lighter than 1 TeV or the longitudinal components of the $W^{\pm}$ and Z bosons interact strongly at center of mass energies of order 1 TeV or more.[3] Strongly interacting W and Z bosons would be signaled by enhanced production of longitudinally polarized $W^{-}W^{+}$, ZZ, and $W^{\pm}Z$ pairs. If no efficient method is available for determining the polarization of the W and Z bosons, then the standard model process $q_1\bar{q}_2 \rightarrow W^{\pm}Z$, which produces W and Z bosons primarily of transverse polarizations, is an irreducible background to strongly interacting $W^{\pm}Z$ production. The process $q_1\bar{q}_2 \rightarrow W^{\pm}Z$ is also a background to techni-rho

mesons[4] which appear in technicolor models of electroweak symmetry breaking; the techni-rho mesons decay primarily to W^-W^+ and $W^\pm Z$ final states.

In hadron collisions $W^\pm Z$ pairs are produced via quark anti-quark annihilation which proceeds via t- and u-channel quark exchange and s-channel W-boson exchange.[5] Until now $W^\pm Z$ production has been calculated only in the leading-logarithm approximation and the order α_s corrections have only been estimated[6] using the soft-gluon approximation.[7] A complete next-to-leading-logarithm NLL) calculation of hadronic $W^\pm Z$ production is presented in this paper. At the parton level this involves computing the contributions from the $2 \to 3$ real emission processes $q_1\bar{q}_2 \to W^\pm Z g$, $q_1 g \to W^\pm Z q_2$, and $\bar{q}_2 g \to W^\pm Z \bar{q}_1$ as well as the one loop corrections to the $2 \to 2$ process $q_1\bar{q}_2 \to W^\pm Z$.

The NLL calculation presented here makes use of a combination of analytic and Monte Carlo integration methods. The same methods have been used to perform NLL calculations for hadronic ZZ and W^-W^+ production,[8,9] direct photon production,[10] photoproduction,[11] symmetric di-hadron production,[12] and W production.[13] The Monte Carlo approach to NLL calculations has many advantages over a purely analytic calculation. The Monte Carlo approach allows one to calculate any number of observables simultaneously by simply histogramming the appropriate quantities. Futhermore, it is easy to tailor the Monte Carlo calculation to different experimental conditions, for example, detector acceptances, experimental cuts, and jet definitions. Also, with the Monte Carlo approach one can easily study the NLL corrections for different observables, the variation of the NLL corrections in different regions of phase space, and the dependence of the NLL cross section on the choice of scale.

The procedure for the NLL $W^{\pm}Z$ calculation is identical to the procedure used in Refs. 8 and 9 for the NLL ZZ and $W^{-}W^{+}$ calculations, respectively. In fact, most of the expressions for the $W^{\pm}Z$ case can be obtained from the corresponding expressions for the ZZ case by simply replacing the ZZ Born cross section with the $W^{\pm}Z$ Born cross section. The only exception to this rule is the finite virtual correction, which must be calculated anew. Thus only the final expressions for the NLL $W^{\pm}Z$ calculation will be given in this paper. Details on the derivations of these expressions can be found in Ref. 8.

The remainder of this paper is organized as follows. Section 2 describes the techniques used in the Monte Carlo approach to NLL calculations. The NLL calculation of $W^{\pm}Z$ production is described in Section 3. Results are presented in Section 4 and summary remarks are given in Section 5. Finally, there is an appendix containing loop integrals which arise in the calculation of the virtual corrections.

2. MONTE CARLO FORMALISM

The Monte Carlo formalism for NLL calculations has been described in detail in Refs. 8–13 so the discussion here will be brief. The basic challenge is to design a program which retains the versatility inherent in a Monte Carlo approach while ensuring that all of the required cancelations of singularities still takes place. In order to discuss the technique for isolating the various singularities, let the four-vectors of the two-body and three-body subprocesses be labelled by $p_1 + p_2 \rightarrow p_3 + p_4$ and $p_1 + p_2 \rightarrow p_3 + p_4 + p_5$, respectively, and define the Lorentz scalars $s_{ij} = (p_i + p_j)^2$ and $t_{ij} = (p_i - p_j)^2$. The $W^{\pm}Z$ calculation contains infrared (IR) and collinear singularities but no ultraviolet singularities.

Dimensional regularization[14] is used to isolate the singularities. First, three-body phase space is partitioned into singular and finite regions by introducing soft and collinear cut-off parameters, δ_s and δ_c. The soft region of phase space is defined to be the region where the gluon energy in the subprocess rest frame becomes less than $\delta_s\sqrt{s_{12}}/2$. The collinear regions of phase space are defined to be those regions where any invariant (s_{ij} or t_{ij}) becomes smaller in magnitude than $\delta_c\, s_{12}$. Next, the squared three-body matrix elements are approximated in the singular regions; the soft gluon and leading-pole approximations are used in the soft and collinear regions, respectively. The resulting expressions are then integrated over the singular regions of phase space. At this stage the integrated expressions contain finite two-body contributions as well as singular pieces. The singularities from the soft region will cancel the virtual IR singularities while the singularities from the collinear region will be factorized into the parton distribution function. The remainder of three-body phase space contains no singularities and the subprocesses can be evaluated in four dimensions.

The calculation now consists of two pieces – a set of two-body contributions and a set of three-body contributions. Each set consists of finite parts, all singularities having been cancelled or factorized. At this stage both pieces depend on the values chosen for the two theoretical cut-offs δ_s and δ_c so that each piece by itself has no intrinsic meaning. However, when the two- and three-body contributions are combined to form a suitably inclusive observable all dependence on the cut-offs cancels. The cut-offs merely serve to distinguish the regions where the phase space integrations are done by hand from those where they are done by Monte Carlo. When the results are added together, the precise location of the boundary between the two regions is not relevant. The results reported below

are stable to reasonable variations in the cut-offs, thus providing a check on the calculation.

3. NEXT-TO-LEADING-LOGARITHM FORMALISM

3.1 Born process

The Feynman diagrams which contribute to the Born amplitude for the reaction

$$q_1(p_1) + \bar{q}_2(p_2) \longrightarrow W(p_3) + Z(p_4)\,, \tag{1}$$

are shown in Fig. 1. The Born amplitude in N dimensions is

$$\mathcal{M}^{\rm Born} = \delta_{i_1 i_2}\, e^2\, \mu^{4-N}\, V_{q_1 q_2}\, \epsilon^*_\mu(p_3)\, \epsilon^*_\nu(p_4) \sum_{\tau=\pm} g_\tau^{q_2 W q_1}\, \bar{V}(p_2) P_{-\tau} T^{\mu\nu} U(p_1)\,, \tag{2}$$

where $\delta_{i_1 i_2}$ is the color tensor (i_1, i_2 are color indices for quarks 1 and 2), e is the electromagnetic coupling constant, μ is a mass parameter introduced to keep the couplings dimensionless, $V_{q_1 q_2}$ is the Cabibbo-Kobayashi-Maskawa (CKM) quark mixing matrix, $\epsilon^*_\mu(p_3)$ and $\epsilon^*_\nu(p_4)$ are the W- and Z-boson polarization tensors, and P_τ denotes the left- right-projection operator $P_\tau = \frac{1}{2}(1 + \tau\gamma_5)$. In the Feynman gauge the tensor $T^{\mu\nu}$ is

$$\begin{aligned} T^{\mu\nu} = {} & g_\tau^{q_1 Z q_1}\, \gamma^\mu \frac{(\not{p}_1 - \not{p}_4)}{u} \gamma^\nu + g_\tau^{q_2 Z q_2}\, \gamma^\nu \frac{(\not{p}_1 - \not{p}_3)}{t} \gamma^\mu \\ & - (Q_1 - Q_2) \frac{\cot\theta_{\rm W}}{s - M_W^2 + i\Gamma_W M_W} \Big[(\not{p}_3 - \not{p}_4) g^{\mu\nu} + 2p_4^\mu \gamma^\nu - 2p_3^\nu \gamma^\mu \Big]\,, \end{aligned} \tag{3}$$

where Q_1 and Q_2 are the electric charges of quarks 1 and 2 (in units of the proton charge e) and $(Q_1 - Q_2)$ is the charge of the W-boson. The right- and left-handed

weak-boson-to-quark couplings are denoted by $g_{\pm}^{qVq}$,

$$\begin{aligned} g_{-}^{uWd} &= g_{-}^{dWu} = \frac{1}{\sqrt{2}\sin\theta_{\rm w}}\,, & g_{+}^{uWd} &= g_{+}^{dWu} = 0\,, \\ g_{-}^{qZq} &= \frac{T_3^q}{\sin\theta_{\rm w}\cos\theta_{\rm w}} - Q_q\tan\theta_{\rm w}\,, & g_{+}^{qZq} &= -Q_q\tan\theta_{\rm w}\,, \end{aligned} \tag{4}$$

where Q_q and T_3^q denote the electric charge and the third component of weak isospin of quark q, and $\theta_{\rm w}$ is the weak mixing angle. The kinematic invariants s, t, u are defined by

$$s = (p_1 + p_2)^2\,, \qquad t = (p_1 - p_3)^2\,, \qquad u = (p_1 - p_4)^2\,. \tag{5}$$

As explained in Ref. 8 (see also Refs. 15 and 16), the γ_5 matrix can be eliminated from all traces, thus making it straightforward to evaluate the traces in N dimensions. The algebra for this paper was evaluated using the computer algebra program FORM.[17]

The squared amplitude summed over final state polarizations and initial state spins can be written

$$|\mathcal{M}^{\rm Born}|^2 = N_C\, e^4\, \mu^{4\epsilon}\, |V_{q_1 q_2}|^2 \left(g_{-}^{q_2 W q_1}\right)^2 \sum_{i=1}^{6} A_i\, B_i\,, \tag{6}$$

where N_C is the number of colors, A_i contains coupling and propagator factors, B_i are dimensionless functions of the kinematic invariants, and the number of space-time dimensions is $N = 4 - 2\epsilon$. For the process $u\bar{d} \to W^+ Z$ the A_i factors

are

$$
\begin{aligned}
A_1 &= \left(g_-^{uZu}\right)^2 , \qquad A_2 = A_1(u \to d) , \\
A_3 &= \cot^2\theta_{\rm w}\, \frac{s^2}{(s-M_W^2)^2+(\Gamma_W M_W)^2} , \\
A_4 &= g_-^{uZu}\, g_-^{dZd} , \\
A_5 &= -\, g_-^{uZu}\, \cot\theta_{\rm w}\, \frac{s(s-M_W^2)}{(s-M_W^2)^2+(\Gamma_W M_W)^2} , \qquad A_6 = A_5(u \to d) ,
\end{aligned}
\tag{7}
$$

and the B_i expressions are

$$
\begin{aligned}
B_1 = {} & \frac{(tu-M_W^2M_Z^2)}{M_W^2M_Z^2} + (1-\epsilon)\left\{\frac{4}{u^2}(tu-M_W^2M_Z^2) + 2s\left[\frac{1}{M_W^2}+\frac{1}{M_Z^2}\right]\right\} \\
& - \epsilon(1-\epsilon)\frac{4}{u^2}(tu-M_W^2M_Z^2) , \\
B_2 = {} & B_1(t \leftrightarrow u) , \\
B_3 = {} & \frac{(t+u)^2}{s^2}\frac{(tu-M_W^2M_Z^2)}{M_W^2M_Z^2} \\
& + (1-\epsilon)\left\{2\frac{(t+u)^2}{s}\left[\frac{1}{M_W^2}+\frac{1}{M_Z^2}\right] - \frac{8}{s}(M_W^2+M_Z^2) + \frac{8}{s^2}(tu-M_W^2M_Z^2)\right\} , \\
B_4 = {} & -2\frac{(tu-M_W^2M_Z^2)}{M_W^2M_Z^2} + (1-\epsilon)\left\{8\frac{s}{tu}(M_W^2+M_Z^2) - 4s\left[\frac{1}{M_W^2}+\frac{1}{M_Z^2}\right]\right\} \\
& - \epsilon(1-\epsilon)\frac{8}{tu}(tu-M_W^2M_Z^2) , \\
B_5 = {} & -2\frac{(t+u)}{s}\frac{(tu-M_W^2M_Z^2)}{M_W^2M_Z^2} \\
& + (1-\epsilon)\left\{\frac{8}{u}(M_W^2+M_Z^2) - \frac{8}{su}(tu-M_W^2M_Z^2) - 4(t+u)\left[\frac{1}{M_W^2}+\frac{1}{M_Z^2}\right]\right\} , \\
B_6 = {} & -B_5(t \leftrightarrow u) .
\end{aligned}
\tag{8}
$$

For the charge conjugate process $d\bar{u} \to W^-Z$, the A_i factors are obtained by interchanging $u \leftrightarrow d$ and replacing $\cot\theta_{\rm w} \to -\cot\theta_{\rm w}$ in Eq. (7) and the B_i expressions are unchanged.

The Born subprocess cross section is

$$d\hat{\sigma}^{\rm Born}(q_1\bar{q}_2 \to WZ) = \frac{1}{4}\frac{1}{9}\frac{1}{2s}\,|\mathcal{M}^{\rm Born}|^2\,d^N\Phi_2\,, \tag{9}$$

where the factors $\frac{1}{4}$ and $\frac{1}{9}$ are the spin average and color average, respectively, and two-body phase space is

$$d^N\Phi_2 = \frac{1}{8\pi}\left(\frac{4\pi}{s}\right)^{\epsilon}\frac{1}{\Gamma(1-\epsilon)}\left[\lambda(1,\frac{M_W^2}{s},\frac{M_Z^2}{s})\right]^{\frac{1}{2}-\epsilon} v^{-\epsilon}(1-v)^{-\epsilon}\,dv\,, \tag{10}$$

with $v = \frac{1}{2}(1+\cos\theta)$. Here λ is the two-body phase space function

$$\lambda(x,y,z) = x^2+y^2+z^2-2xy-2xz-2yz\,. \tag{11}$$

It is convenient to decompose the squared Born amplitude into three terms corresponding to the power of ϵ that appears in the squared amplitude

$$|\mathcal{M}^{\rm Born}|^2 = |\mathcal{M}_0^{\rm Born}|^2 + \epsilon|\mathcal{M}_1^{\rm Born}|^2 + \epsilon^2|\mathcal{M}_2^{\rm Born}|^2\,, \tag{12}$$

with this decomposition the Born cross section can be written

$$d\hat{\sigma}^{\rm Born} = d\hat{\sigma}_0^{\rm Born} + \epsilon\,d\hat{\sigma}_1^{\rm Born} + \epsilon^2 d\hat{\sigma}_2^{\rm Born}\,. \tag{13}$$

This decomposition will be useful later for writing the virtual and soft corrections.

The leading-logarithm (LL) cross section is obtained by convoluting the subprocess cross section with the parton densities and summing over the contributing partons,

$$\begin{aligned}\sigma^{\rm LL}(pp\to WZ) = \sum_{q_1,\bar{q}_2}\int & d\hat{\sigma}^{\rm Born}(q_1\bar{q}_2\to WZ) \\ & \times\Big[G_{q_1/p}(x_1,M^2)G_{\bar{q}_2/p}(x_2,M^2) + x_1\leftrightarrow x_2\Big]dx_1dx_2\,.\end{aligned} \tag{14}$$

3.2 Virtual Processes

The order α_s virtual correction to $q_1\bar{q}_2 \to WZ$ comes from the interference between the Born graphs of Fig. 1 and the virtual graphs shown in Fig. 2. The interference between these amplitudes has been evaluated in N dimensions using the Feynman parameterization technique. There are two mitigating factors which simplify the $q_1\bar{q}_2 \to WZ$ virtual calculation. The first is that the calculation does not contain UV singularities since the graphs in Fig. 2 do not contribute to the renormalization of the strong, electromagnetic, or weak coupling constants. The second is that the self-energy insertions on the external quark lines vanish due to the cancellation of the UV and IR divergences.[18] Basically, what happens is that the UV and IR poles cancel when one does not distinguish between them.

Because the loop integrals associated with the four-point function from the box diagrams in Fig. 2 are very difficult to evaluate when powers of the loop momenta appear in the numerator, it is advantageous to first multiply the Born amplitudes times the virtual amplitudes and evaluate the resulting traces. The numerator of the resulting expression can then be rewritten, using momentum conservation relations, such that propagator denominator factors cancel with identical factors in the numerator. This way the four-point functions with powers of the loop momentum in the numerator are reduced to a four-point function with a constant numerator and three- and two-point functions which are easier to evaluate. The loop integrals can be reduced to a set of twelve integrals which were given in Refs. 8 and 9 for the case of equal mass weak bosons. For the present case of unequal mass weak bosons, four of the twelve integrals must be generalized and are given in an appendix.

The order α_s virtual contribution to the $q_1\bar{q}_2 \to WZ$ cross section is

$$\frac{d\hat{\sigma}^{\rm virt}}{dv} = C_F \frac{\alpha_s}{2\pi}\left(\frac{4\pi\mu^2}{s}\right)^{\epsilon}\frac{\Gamma(1-\epsilon)}{\Gamma(1-2\epsilon)}\left\{ -\frac{2}{\epsilon^2}\frac{d\hat{\sigma}_0^{\rm Born}}{dv} - \frac{2}{\epsilon}\frac{d\hat{\sigma}_1^{\rm Born}}{dv} - \frac{3}{\epsilon}\frac{d\hat{\sigma}_0^{\rm Born}}{dv} \right.$$
$$\left. + \frac{1}{4}\frac{1}{9} N_C\, e^4\, |V_{q_1 q_2}|^2 \left(g_-^{q_2 W q_1}\right)^2 \sum_{i=1}^{6} A_i\, V_i \right\}, \tag{15}$$

where $d\hat{\sigma}_0^{\rm Born}$ and $d\hat{\sigma}_1^{\rm Born}$ are defined by Eq. (13) and $C_F = \frac{4}{3}$ is the quark-gluon vertex color factor. In the last term, which is the order α_s finite virtual correction, the A_i are the coupling factors defined in Eq. (7) and the V_i are dimensionless functions of the kinematic invariants. The V_i expressions are too lengthy to reproduce here, however, to facilitate future comparisons with the present calculation, the finite virtual contribution to the NLL cross section will be plotted in the results section.

3.3 Soft Gluon Emission

The Feynman diagrams for the real emission subprocess

$$q_1(p_1) + \bar{q}_2(p_2) \longrightarrow W(p_3) + Z(p_4) + g(p_5)\,, \tag{16}$$

are shown in Fig. 3. In the soft gluon region of three-body phase space, which is defined by $E_5 < \delta_s \sqrt{s_{12}}/2$, the soft gluon contribution to the cross section is

$$\frac{d\hat{\sigma}^{\rm soft}}{dv} = C_F \frac{\alpha_s}{2\pi}\left(\frac{4\pi\mu^2}{s}\right)^{\epsilon}\frac{\Gamma(1-\epsilon)}{\Gamma(1-2\epsilon)}$$
$$\times \left[\frac{2}{\epsilon^2}\frac{d\hat{\sigma}_0^{\rm Born}}{dv} + \frac{2}{\epsilon}\left\{-2\log(\delta_s)\frac{d\hat{\sigma}_0^{\rm Born}}{dv} + \frac{d\hat{\sigma}_1^{\rm Born}}{dv}\right\} \right. \tag{17}$$
$$\left. + 4\log(\delta_s)^2\frac{d\hat{\sigma}_0^{\rm Born}}{dv} - 4\log(\delta_s)\frac{d\hat{\sigma}_1^{\rm Born}}{dv} + 2\frac{d\hat{\sigma}_2^{\rm Born}}{dv}\right],$$

where δ_s is the soft cut-off parameter defined in Sec. 2.

3.4 Hard Collinear Corrections

The $2 \to 3$ real emission processes have hard collinear singularities when $t_{15} \to 0$ or $t_{25} \to 0$. These singularities must be factorized and absorbed into the initial state parton distribution functions. The collinear regions of three-body phase space are defined to be those regions where any invariant (s_{ij} or t_{ij}) becomes smaller in magnitude than $\delta_c s_{12}$, where δ_c is the collinear cut-off parameter defined in Sec. 2. After the factorization is performed, the remnants of the hard collinear singularities take the form

$$\begin{aligned}\frac{d\tilde{\sigma}}{dv}(q_1\bar{q}_2 \to WZ) = &\frac{\alpha_s}{2\pi}\frac{d\hat{\sigma}_0^{\rm Born}}{dv} \\ &\times \Bigg[\; G_{q_1/p}(x_1,M^2)\int_{x_2}^{1-\delta_s}\frac{dz}{z}\,G_{\bar{q}_2/p}(\frac{x_2}{z},M^2)\,\tilde{P}_{qq}(z) \\ &+ G_{q_1/p}(x_1,M^2)\int_{x_2}^{1}\frac{dz}{z}\,G_{g/p}(\frac{x_2}{z},M^2)\,\tilde{P}_{qg}(z) \\ &+ G_{\bar{q}_2/p}(x_2,M^2)\int_{x_1}^{1-\delta_s}\frac{dz}{z}\,G_{q_1/p}(\frac{x_1}{z},M^2)\,\tilde{P}_{qq}(z) \\ &+ G_{\bar{q}_2/p}(x_2,M^2)\int_{x_1}^{1}\frac{dz}{z}\,G_{g/p}(\frac{x_1}{z},M^2)\,\tilde{P}_{qg}(z)\Bigg] ,\end{aligned} \tag{18}$$

with

$$\tilde{P}_{ij}(z) \equiv P_{ij}(z)\,\ln\Big(\frac{1-z}{z}\,\delta_c\,\frac{s}{M^2}\Big) - P'_{ij}(z) - \lambda_{FC}F_{ij}(z)\,. \tag{19}$$

The Altarelli-Parisi splitting functions in $N = 4 - 2\epsilon$ dimensions for $0 < z < 1$

are

$$P_{qq}(z,\epsilon) = C_F \left[\frac{1+z^2}{1-z} - \epsilon(1-z)\right] ,$$
$$P_{qg}(z,\epsilon) = \frac{1}{2(1-\epsilon)} \left[z^2 + (1-z)^2 - \epsilon\right] , \tag{20}$$

and can be written

$$P_{ij}(z,\epsilon) = P_{ij}(z) + \epsilon P'_{ij}(z) , \tag{21}$$

which defines the P'_{ij} functions. The functions F_{qq} and F_{qg} depend on the choice of factorization convention and the parameter λ_{FC} specifies the factorization convention; $\lambda_{FC} = 0$ for the universal ($\overline{\rm MS}$) convention and $\lambda_{FC} = 1$ for the physical (Deep Inelastic Scattering DIS) convention. For the physical convention the factorization functions are

$$F_{qq}(z) = C_F \left[\frac{1+z^2}{1-z} \ln\left(\frac{1-z}{z}\right) - \frac{3}{2}\frac{1}{1-z} + 2z + 3\right] ,$$
$$F_{qg}(z) = \frac{1}{2} \left[\left\{z^2 + (1-z)^2\right\} \ln\left(\frac{1-z}{z}\right) + 8z(1-z) - 1\right] . \tag{22}$$

The parameter M^2 is the factorization scale which must be specified in the process of factorizing the collinear singularity. Basically, it determines how much of the collinear term is absorbed into the various parton distributions.

The upper limit on the integrals appearing in Eq. (18) is determined by requiring that the hard collinear term not overlap with the soft region previously discussed. If such an overlap were to occur, then that region of three-body phase space would be counted twice.

3.5 Soft Collinear Subtraction Term

The M^2 dependent subtraction piece which is used to absorb the collinear singularity into the parton distribution functions involves an integral over splitting functions with the upper limit corresponding to $z = 1$, not $1 - \delta_s$. Therefore, there is one last piece to be subtracted which, for the t_{15} case, takes the form

$$\begin{aligned}\frac{d\hat{\sigma}^{15}}{dv} = \frac{d\hat{\sigma}^{\rm Born}}{dv}\,\frac{\alpha_s}{2\pi}\left(\frac{4\pi\mu^2}{M^2}\right)^{\epsilon}\frac{\Gamma(1-\epsilon)}{\Gamma(1-2\epsilon)} \\ \times\int_{1-\delta_s}^{1}\frac{dz}{z}\left\{-\frac{1}{\epsilon}P_{qq}(z)+\lambda_{FC}F_{qq}(z)\right\}G_{q/p}\left(\frac{x}{z}\right).\end{aligned} \tag{23}$$

Inserting P_{qq} and F_{qq} and integrating yields

$$\begin{aligned}\frac{d\hat{\sigma}^{15}}{dv} = -\,C_F\,\frac{\alpha_s}{2\pi}\left(\frac{4\pi\mu^2}{s}\right)^{\epsilon}\frac{\Gamma(1-\epsilon)}{\Gamma(1-2\epsilon)}\left[\frac{1}{\epsilon}\left\{\frac{3}{2}+2\log(\delta_s)\right\}\frac{d\hat{\sigma}_0^{\rm Born}}{dv}\right. \\ +\left\{\frac{3}{2}+2\log(\delta_s)\right\}\left\{\log\left(\frac{s}{M^2}\right)\frac{d\hat{\sigma}_0^{\rm Born}}{dv}+\frac{d\hat{\sigma}_1^{\rm Born}}{dv}\right\} \\ \left.+\,\lambda_{FC}\left\{\frac{9}{2}+\frac{\pi^2}{3}+\frac{3}{2}\log(\delta_s)-\log(\delta_s)^2\right\}\frac{d\hat{\sigma}_0^{\rm Born}}{dv}\right],\end{aligned} \tag{24}$$

where terms proportional to a power of the soft cut-off δ_s have been discarded. The soft collinear singularity in the $t_{25} \to 0$ region yields an identical result.

3.6 Next-to-Leading-Logarithm Cross Section

The NLL cross section, which consists of two- and three-body contributions, can now be assembled from the pieces described in the previous sections. The

two-body contribution is

$$\sigma_{2\text{ body}}^{\text{NLL}}(pp \to WZ) = \sum_{q_1,\bar{q}_2} \int dv\, dx_1\, dx_2 \qquad (25)$$
$$\times \left[G_{q_1/p}(x_1, M^2)\, G_{\bar{q}_2/p}(x_2, M^2)\, \frac{d\hat{\sigma}^{\text{NLL}}}{dv}(q_1\bar{q}_2 \to WZ) + (x_1 \leftrightarrow x_2) + \frac{d\tilde{\sigma}}{dv} \right],$$

where the sum is over all contributing quark flavors, $d\tilde{\sigma}/dv$ is defined in Eq. (18), and

$$\frac{d\hat{\sigma}^{\text{NLL}}}{dv}(q_1\bar{q}_2 \to WZ) = \frac{d\hat{\sigma}^{\text{Born}}}{dv} + \frac{d\hat{\sigma}^{\text{virt}}}{dv} + \frac{d\hat{\sigma}^{\text{soft}}}{dv} - \frac{d\hat{\sigma}^{15}}{dv} - \frac{d\hat{\sigma}^{25}}{dv}\,. \qquad (26)$$

The $\frac{1}{\epsilon^2}$ and $\frac{1}{\epsilon}$ poles cancel when the terms in Eq. (26) are summed [see Eqs. (9), (15), (17), and (24)].

The three-body contribution to the cross section is

$$\sigma_{3\text{ body}}(pp \to WZ + X) = \sum_{a,b,c} \int d\hat{\sigma}(ab \to WZc)$$
$$\times \Big[G_{a/p}(x_1, M^2)\, G_{b/p}(x_2, M^2) + (x_1 \leftrightarrow x_2) \Big] dx_1\, dx_2\,, \qquad (27)$$

where the sum is over all partons contributing to the three subprocesses $q_1\bar{q}_2 \to WZg$, $q_1 g \to WZq_2$, and $\bar{q}_2 g \to WZq_1$. The squared matrix elements for the $2 \to 3$ subprocesses were evaluated numerically via helicity amplitude methods as described in Ref. 19. The integration over three-body phase space and $dx_1\, dx_2$ is done numerically by standard Monte Carlo techniques. The kinematic invariants s_{ij} and t_{ij} are first tested for soft and collinear singularities. If an invariant for a subprocess falls in a soft or collinear region of phase space, the contribution from that subprocess is not included in the cross section.

4. RESULTS

The numerical results presented in this section have been obtained using the two-loop expression for α_s. The QCD scale $\Lambda_{\rm QCD}$ is specified for four flavors of quarks by the choice of parton distribution functions and is adjusted whenever a heavy quark threshold is crossed so that α_s is a continuous function of Q^2. The heavy quark masses were taken to be $m_b = 5$ GeV and $m_t = 140$ GeV (Ref. 20). The standard model parameters were taken to be $M_Z = 91.17$ GeV, $M_W = 80.0$ GeV, and $\alpha(M_W) = 1/128$. These mass values are consistent with recent measurements at the Tevatron,[21] the SLAC Linear Collider,[22] and the CERN e^+e^- collider LEP.[23] The soft and collinear cut-off parameters were taken to be $\delta_s = 5 \times 10^{-2}$ and $\delta_c = 10^{-3}$. The parton subprocesses have been summed over u, d, c, and s quarks and the Cabibbo mixing angle has been chosen such that $\cos^2\theta_C = 0.95$. Except where otherwise stated, a single scale $Q^2 = M_{WZ}^2$, where M_{WZ} is the invariant mass of the WZ pair, has been used for the renormalization scale μ^2 and factorization scale M^2. For comparison, LL predictions obtained with the two-loop running coupling for α_s are also given. Using the two-loop running coupling for both the LL and NLL results provides a consistent expansion parameter so that one can judge the degree of convergence of the results. The results presented here for $W^\pm Z$ production are qualitatively similar to the results for ZZ and W^-W^+ production.[8,9]

In order to get consistent NLL results it is necessary to use parton distribution functions which have been fit to next-to-leading order. The dependence of the total cross section on the choice of parton distribution functions is shown in Table 1 where the total cross section for W^+Z production at the Tevatron, LHC, and SSC are given for the HMRS[24] sets E and B and for the DFLM[25]

sets corresponding to $\Lambda_4 = 160$, 260, and 360 MeV. The variation in the cross section increases with the center of mass energy; at the SSC energy the ratio of the extreme values for the cross section is 1.8 (1.4 if the HMRS set E distributions are disregarded). The HMRS set B distributions will be used for the remainder of this section since they fit the present data the best. Note that the HMRS distributions are defined in the universal ($\overline{\rm MS}$) scheme whereas the DFLM distributions are defined in the physical (DIS) scheme. The factorization defining parameter λ_{FC} in Eqs. (19) and (24) should thus be $\lambda_{FC} = 0\,(1)$ for the HMRS (DFLM) distributions.

One of the motivations for performing NLL calculations is that the results often show a less dramatic dependence on the renormalization and factorization scale than the LL result. This is true for the present calculation. The scale dependence of the total cross section is illustrated in Fig. 4 where the total cross section for W^+Z production is plotted verses the scale Q. The scale Q has been used for both the renormalization and factorization scales. Parts a), b), and c) of Fig. 4 are for the Tevatron, LHC, and SSC, respectively. The NLL result at the Tevatron shows only a slight decrease in scale dependence, while the NLL results at the LHC and SSC show a significant decrease in scale dependence. The qualitative differences between the results at the Tevatron and SSC are due to the differences between $p\bar{p}$ verses pp scattering and the ranges of the x-values. At the Tevatron, W^+Z production in $p\bar{p}$ collisions is dominated by valence quark interactions. The valence quark distributions decrease with Q^2 for the x-values probed at the Tevatron. On the other hand, at the LHC and SSC, sea quark interactions dominate in the pp process and smaller x-values are probed. The sea quark distributions increase with Q^2 for the x-values probed by the LHC and

SSC. Thus the cross section decreases with Q^2 at the Tevatron but increases with Q^2 at the SSC. At the LHC the NLL cross section is nearly independent of Q^2 because the increasing parton distributions are compensated by the decreasing of α_s.

The NLL and LL total cross sections for $pp \to W^{\pm}Z$ are plotted in Fig. 5 as functions of the center of mass energy. The order α_s corrections are positive and enhance the lowest order cross section by 30-70% over the range of center of mass energies shown in the figure. Also shown in Fig. 5 is the LL result with a multiplicative soft-gluon K-factor. The soft-gluon K-factor is a scheme dependent approximation for the order α_s corrections. In the $\overline{\rm MS}$ scheme, which is used for the figures in this paper, the soft-gluon K-factor is $K = 1+\frac{4\pi}{9}\alpha_s$ (Ref. 6); in the DIS scheme the α_s term is twice the size as in the $\overline{\rm MS}$ scheme. Figure 5 shows that the soft-gluon K-factor underestimates the order α_s corrections; the underestimation gets worse as the center of mass energy increases. The soft-gluon K-factor is a better estimate in the DIS scheme because it is twice as large, but it still underestimates the complete NLL cross section. Note also that the K-factor simply enhances the LL cross section uniformly over the entire range of center of mass energies, whereas the complete order α_s corrections increase with the center of mass energy. The short-comings of the soft-gluon K-factor are linked to the fact that it only approximates the order α_s $q\bar{q}$ corrections in the limit of soft virtual and real gluon emissions. The presence of large order α_s qg initiated processes (see next paragraph) invalidates the use of the soft-gluon K-factor. A comparison with the complete order α_s $q\bar{q}$ corrections shows that it also underestimates them by 50% (25%) in the $\overline{\rm MS}$ (DIS) scheme. At the SSC center of mass energy, the order α_s corrections enhance the lowest order cross

section for $W^{\pm}Z$ production by a factor of 1.7. For comparison, the order α_s corrections yield enhancement factors of 1.5 for W^-W^+ production[9] and 1.3 for ZZ production.[8] In contrast, the soft-gluon K-factor is the same in all three cases[6] and yields an enhancement factor of approximately 1.13 (1.26) in the $\overline{\rm MS}$ (DIS) scheme.

To understand why the order α_s corrections differ for the cases of ZZ, W^-W^+, and $W^{\pm}Z$ production, Fig. 6 shows the NLL total cross section for $W^{\pm}Z$ production decomposed into the LL contribution and the order α_s contributions from $q\bar{q}$ and qg initial states. The order α_s corrections from $q\bar{q}$ initial states are approximately 35% as large as the LL cross section for the entire range of center of mass energies shown in the figure, however, the corrections from qg initial states increase from -1% to 35% as large as the LL cross section as the center of mass energy increases. Similar figures for hadronic ZZ and W^-W^+ production show that the order α_s $q\bar{q}$ corrections are similar in all three cases, but that the order α_s qg corrections increase as one goes from ZZ to W^-W^+ to $W^{\pm}Z$. A similar behavior is observed in the tree-level $VV+1$ jet cross section ($VV = ZZ, W^-W^+, W^{\pm}Z$); the qg initial state component of the cross section increases as one goes from ZZ to W^-W^+ to $W^{\pm}Z$. The fraction of cross section with both weak bosons in the same hemisphere also increases in the same order. The processes with non-abelian graphs (W^-W^+ and $W^{\pm}Z$) are enhanced when both weak bosons are in the same hemisphere. This configuration minimizes the invariant mass of the weak boson pair which in turn puts the propagator closer to its on-shell value. This enhancement is most pronounced for the $W^{\pm}Z$ case; the W^-W^+ case suffers from destructive interference between the virtual photon and virtual Z-boson graphs. Thus the W^-W^+ case is intermediate between the

ZZ and $W^{\pm}Z$ case. The enhancement is also more pronounced in the qg channel than in the $q\bar{q}$ channel. The increase in the size of the order α_s corrections is due to the increasing importance of the qg initial state contribution.

To facilitate future comparisons with the present calculation, Fig. 7 shows the order α_s finite virtual correction from Eq. (15). This correction is positive and about an order of magnitude smaller than the LL cross section.

One of the major advantages of using Monte Carlo methods for NLL calculations is that one can calculate any number of differential distributions simultaneously by simply histogramming the quantity of interest. Figures 8, 9, and 10 show the differential distributions for the WZ pair invariant mass M_{WZ}, the Z-boson transverse momentum $p_T(Z)$, and the Z-boson rapidity in the laboratory frame $y(Z)$, respectively, for $pp \to W^+Z$ at the LHC and SSC center of mass energies. No cuts have been applied to these figures. Because of the mass difference between the Z- and W-bosons, the $y(W)$ distribution is slightly broader than the $y(Z)$ distribution and the $p_T(W)$ distribution is slightly higher (lower) at small (large) values of transverse momentum than the $p_T(Z)$ distribution. These figures show that the order α_s corrections are larger at large p_T, large M_{WZ}, and small y values. Thus in general, the order α_s corrections do not simply change the overall normalizations, but instead they also change the shapes of kinematic distributions. These shape changes are due to the presence of three-body final states in the order α_s cross section. Two-body phase space is a highly constrained configuration, whereas three-body phase space allows many new configurations, for example, both the W- and Z-boson can be in the same hemisphere. A comparison between the two-body tree-level process $pp \to WZ$ and the three-body tree-level process $pp \to WZ + 1$ jet, shows that the $p_T(Z)$

spectrum is harder in the latter process. Examination of the two- and three-body contributions to the NLL $p_T(Z)$ distribution indeed shows that the high-$p_T(Z)$ tail is dominated by the three-body contribution. By contrast, the soft-gluon K-factor simply scales up the lowest order cross section and predicts no shape change in the kinematic distributions. The K-factor's lack of shape change is understandable since the soft-gluon limit is a two-body final state whereas three-body final states are needed to produce a change in shape.

5. SUMMARY

A complete next-to-leading-logarithm calculation of $p\overset{(-)}{p} \to W^{\pm}Z$ has been presented. The calculation was done using a combination of analytic and Monte Carlo integration methods which make it easy to calculate a variety of observables and to impose experimental cuts. The order α_s corrections enhance the lowest order cross section by 30-70%. The size of the NLL corrections depends on the observable and on the kinematic range. The NLL results are less dependent on the scale choice than the LL result, especially at supercollider energies. These results are qualitatively similar to the results for hadronic ZZ and W^-W^+ production, however, the processes $pp \to ZZ$, W^-W^+, and $W^{\pm}Z$ have progressively larger order α_s corrections.

ACKNOWLEDGEMENTS

The author wishes to thank H. Baer, U. Baur, and T. Han for useful discussions. Special thanks go to J. F. Owens for advice during the course of this project and for reading this manuscript. The author also wishes to thank the Fermilab theory group for hospitality and support while this work was being completed. This research was supported in part by the U. S. Department of Energy under contract number DE-FG05-87-ER40319.

APPENDIX : LOOP INTEGRALS

The loop integrals from the virtual graphs of Fig. 2 can be reduced to a set of twelve integrals which were given in Refs. 8 and 9 for the case of equal mass weak bosons. For the present case of unequal mass weak bosons, four of the integrals must be generalized and are given in this appendix. The notation here is the same as in Ref. 8.

Three of the integrals (I_5, I_6, and I_7) are infrared and ultraviolet finite and can be evaluated in 4 dimensions, however, the fourth integral (I_1) is singular and must be regularized. Dimensional regularization was used to regularize this integral, with the number of space-time dimensions set to $N = 4 - 2\epsilon$. In all cases the integrals were evaluated using the Feynman parameterization technique. Integrals $I_5^{\mu\nu}$ and I_6^{μ} are only needed for the cases in which the indices are contracted with $p_{1\mu}p_{1\nu}$ and $p_{1\mu}$, respectively. The integrals are written with a common factor

$$F = \left(\frac{4\pi}{s}\right)^{\epsilon} \frac{\Gamma(1-\epsilon)}{\Gamma(1-2\epsilon)} \frac{1}{(4\pi)^2} \,. \tag{A1}$$

The singular integral is

$$\begin{aligned} I_1 &\equiv \int \frac{d^N k}{(2\pi)^N} \frac{1}{k^2(k+p_1)^2(k+p_1-p_3)^2(k-p_2)^2} \qquad (A2) \\ &= i\frac{F}{st}\left[\frac{1}{\epsilon^2} + \frac{2}{\epsilon}\log(\frac{M_W M_Z}{-t}) + \frac{2\pi^2}{3} - 2B_1(t,u)\right] , \end{aligned}$$

where

$$
\begin{aligned}
B_1(t,u) = \quad & \mathrm{Li}_2(\frac{M_Z^2-u}{s}) - \mathrm{Li}_2(\frac{s-M_W^2}{s}) \\
& - \mathrm{Li}_2(\frac{-st}{[s-M_W^2][M_W^2-t]}) + \mathrm{Li}_2(\frac{-t}{s-M_W^2}) + \mathrm{Li}_2(\frac{M_Z^2}{M_Z^2-t}) \qquad (A3) \\
& - \tfrac{1}{2}\log(\frac{-st}{[s-M_W^2][M_W^2-t]})^2 + \tfrac{1}{2}\log(\frac{-t}{s-M_W^2})^2 \\
& + \log(\frac{M_W^2-t}{s})\log(\frac{M_Z^2-u}{-t}) - \tfrac{1}{2}\log(\frac{M_W^2-t}{s})\log(\frac{sM_Z^2}{t^2}) - \tfrac{1}{4}\log(\frac{sM_Z^2}{t^2})^2 \\
& + \tfrac{1}{4}\log(\frac{M_W^2}{s})^2 + \tfrac{1}{2}\log(\frac{M_Z^2}{s})\log(\frac{M_W^2-t}{M_W^2}) + \tfrac{1}{2}\log(\frac{M_Z^2}{M_Z^2-t})^2 \,,
\end{aligned}
$$

and $\mathrm{Li}_2(z)$ is the dilogarithm function

$$
\mathrm{Li}_2(z) = -\int_0^1 \log(1-tz)\frac{dt}{t} = \sum_{k=1}^{\infty}\frac{z^k}{k^2}\,. \qquad (A4)
$$

The three finite integrals are

$$
\begin{aligned}
p_{1\mu}p_{1\nu}I_5^{\mu\nu} &\equiv p_{1\mu}p_{1\nu}\int \frac{d^Nk}{(2\pi)^N}\,\frac{k^\mu k^\nu}{(k+p_1)^2(k+p_1-p_3)^2(k-p_2)^2} \qquad (A5) \\
&= i\frac{Fs}{4}\left[\frac{(M_W^2-t)^2}{s^2}J_0 + 2\frac{(M_W^2-t)}{s}J_1 + J_2\right], \\
p_{1\mu}I_6^{\mu} &\equiv p_{1\mu}\int \frac{d^Nk}{(2\pi)^N}\,\frac{k^\mu}{(k+p_1)^2(k+p_1-p_3)^2(k-p_2)^2} \qquad (A6) \\
&= i\frac{F}{2}\left[\frac{(M_W^2-t)}{s}J_0 + J_1\right], \\
I_7 &\equiv \int \frac{d^Nk}{(2\pi)^N}\,\frac{1}{(k+p_1)^2(k+p_1-p_3)^2(k-p_2)^2} = i\,\frac{F}{s}\,J_0\,, \qquad (A7)
\end{aligned}
$$

where the J_i are dimensionless functions defined by

$$J_0 \equiv \int_0^1 \frac{C}{A}\, dz\,, \tag{A8}$$

$$J_1 \equiv -\int_0^1 \left(\frac{\left[M_W^2 - t\right]}{s} - z\right)\left(\frac{1}{A} - \frac{BC}{A^2}\right) dz\,, \tag{A9}$$

$$J_2 \equiv \int_0^1 \left(\frac{\left[M_W^2 - t\right]}{s} - z\right)^2 \left(\frac{1}{2A} - \frac{B}{A^2} + \frac{B^2 C}{A^3}\right) dz\,, \tag{A10}$$

with

$$A = -(z - z_-)(z - z_+)\,, \tag{A11}$$

$$B = \frac{M_W^2}{s} + \frac{(M_Z^2 - M_W^2)}{s} z\,, \tag{A12}$$

$$C = \log(z) + \log(1 - z) - \log(B)\,, \tag{A13}$$

$$z_\pm = \frac{1}{2}\left[1 + \frac{M_W^2}{s} - \frac{M_Z^2}{s} \pm \lambda\left(1, \frac{M_W^2}{s}, \frac{M_Z^2}{s}\right)^{\frac{1}{2}}\right]. \tag{A14}$$

Here λ is the two-body phase space function defined in Eq. (11). The J_i integrals can be evaluated by partial fractioning the denominators and integrating term-by-term. The resulting integrals can be found in the table of integrals by Devoto and Duke[26] and are expressed in terms of logarithm and dilogarithm functions. This process is easily done with the aid of a computer algebra program, however, the resulting expressions for J_i are too lengthy to reproduce here.

REFERENCES

1) E. Eichten, I. Hinchliffe, K. Lane, and C. Quigg, Rev. Mod. Phys. **56**, 579 (1984); **58**, 1065(E) (1986).

2) M. Kuroda, J. Maalampi, K. H. Schwarzer, and D. Schildknecht, Nucl. Phys. **B284**, 271 (1987); D. Zeppenfeld and S. Willenbrock, Phys. Rev. **D37**, 1775 (1988); S.-C. Lee and W.-C. Su, Phys. Lett. **B212**, 113 (1988); K. Hagiwara, J. Woodside, and D. Zeppenfeld, Phys. Rev. **D41**, 2113 (1990); H. Plothow-Besch *et al.*, in *Proceedings of the ECFA Workshop on LHC Physics*, Aachen, FRG, 1990, and also as CERN report No. CERN-PPE/91-38, 1991.

3) D. Dicus and V. Mathur, Phys. Rev. **D7**, 3111 (1973); M. Veltman, Acta Phys. Pol. **B8**, 475 (1977); B. W. Lee, C. Quigg, and H. Thacker, Phys. Rev. **D16**, 1519 (1977); J. van der Bij and M. Veltman, Nucl. Phys. **B231**, 205 (1984); M. S. Chanowitz and M. K. Gaillard, Nucl. Phys. **B216**, 379 (1985).

4) J. Bagger, T. Han, and R. Rosenfeld, Fermilab report No. FERMILAB-CONF-90/253-T, 1990, to appear in *Proceedings of the Summer Study on Research Directions for the Decade*, Snowmass, Colorado, 1990.

5) R. W. Brown, K. O. Mikaelian, and D. Sahdev, Phys. Rev. **D20**, 1164 (1979).

6) V. Barger, J. L. Lopez, and W. Putikka, Int. J. Mod. Phys. **A3**, 2181 (1988).

7) A. P. Contogouris, S. Papadopoulos, and J. P. Ralston, Phys. Rev. **D25**, 1280 (1982); A. P. Contogouris, H. Tanaka, Phys. Rev. **D33**, 1265 (1986); N. Mebarki and H. Tanaka, Mod. Phys. Lett. **2A**, 735 (1987).

8) J. Ohnemus and J. F. Owens, Phys. Rev. **D43**, 3626 (1991). Note that the soft-gluon K-factor used in this reference was incorrectly given in the DIS scheme whereas it should have been given in the $\overline{\rm MS}$ scheme.

9) J. Ohnemus, Florida State University report No. FSU-HEP-910320, 1991, to appear in Phys. Rev. **D**.

10) H. Baer, J. Ohnemus, and J. F. Owens, Phys. Rev. **D42**, 61 (1990); Phys. Lett. **B234**, 127 (1990).

11) H. Baer, J. Ohnemus, and J. F. Owens, Phys. Rev. **D40**, 2844 (1989).

12) L. Bergmann, Ph.D. dissertation, Florida State University, report No. FSU-HEP-890215, 1989 (unpublished).

13) H. Baer and M. H. Reno, Phys. Rev. **D43**, 2892 (1991).

14) G. 't Hooft and M. Veltman, Nucl. Phys. **B44**, 189 (1972).

15) J. Smith, D. Thomas, and W. van Neervan, Z. Phys. **C44**, 267 (1989).

16) B. Mele, P. Nason, and G. Ridolfi, CERN report No. CERN-TH-5890/90, 1990.

17) FORM is a computer algebra program written by J. A. M. Vermaseren (unpublished).

18) W. L. Van Neerven, Nucl. Phys. **B268**, 453 (1986).

19) V. Barger, T. Han, J. Ohnemus, and D. Zeppenfeld, Phys. Rev. **D41**, 2782 (1990).

20) Recent measurements of the Z widths and the W and Z masses indicate that the top quark mass is most likely to be around 140 GeV. See, for example, U. Amaldi, A. Böhm, L. S. Durkin, P. Langacker, A. K. Mann, W. J. Marciano, A. Sirlin, and H. H. Williams, Phys. Rev. **D36**, 1385 (1987); G. Costa, J. Ellis, G. L. Fogli, D. V. Nanopoulos, and F. Zwirner, Nucl. Phys. **B297**, 244 (1988); J. Ellis and G. Fogli, Phys. Lett. **B213**, 526 (1989); V. Barger, J. Hewett, and T. Rizzo, Phys. Rev. Lett. **65**, 1313 (1990).

21) CDF Collaboration, F. Abe *et al.*, Phys. Rev. Lett. **63**, 720 (1989).

22) Mark II Collaboration, G. S. Abrams *et al.*, Phys. Rev. Lett. **63**, 724 (1989).

23) ALEPH Collaboration, D. Decamp *et al.*, Phys. Lett. **B231**, 519 (1989); **235**, 399 (1990); DELPHI Collaboration, P. Aarnio *et al.*, *ibid.* **231**, 539 (1989); L3 Collaboration, B. Adeva *et al.*, *ibid.* **231**, 509 (1989); OPAL Collaboration, M. Z. Akrawy *et al.*, *ibid.* **231**, 530 (1989).

24) P. N. Harriman, A. D. Martin, R. G. Roberts, and W. J. Stirling, Phys. Rev. **D42**, 798 (1990).

25) M. Diemoz, F. Ferroni, E. Longo, and G. Martinelli, Z. Phys. **C39**, 21 (1988).

26) A. Devoto and D. W. Duke, Revista Nuovo Cimento Vol. 7, No. 6, 1 (1984).

Table 1. Predicted cross sections (in pb) for W^+Z production with no cuts at various colliders and for different sets of parton distribution functions.

collider	$\sqrt{s}$ (TeV)		HMRSE	HMRSB	DFLM160	DFLM260	DFLM360
Tevatron	1.8	LL	1.09	1.01	0.941	0.868	0.806
Tevatron	1.8	NLL	1.42	1.33	1.29	1.21	1.14
LHC	16.	LL	14.4	16.8	17.0	18.2	19.0
LHC	16.	NLL	21.8	25.6	27.0	29.2	30.6
SSC	40.	LL	33.9	43.1	43.7	51.2	58.1
SSC	40.	NLL	55.9	71.3	74.5	87.8	99.6

FIGURE CAPTIONS

1. Feynman diagrams for the Born subprocess $q_1\bar{q}_2 \to WZ$. The straight, wavy, and curly lines denote quarks, electroweak bosons, and gluons, respectively.

2. Feynman diagrams for the virtual subprocess $q_1\bar{q}_2 \to WZ$. Not shown are the diagrams obtained by interchanging the W and Z.

3. Feynman diagrams for the real emission subprocess $q_1\bar{q}_2 \to WZg$. Not shown are the diagrams obtained by interchanging the W and Z.

4. Total cross section for W^+Z production as a function of the scale Q. The solid curve is the NLL result and the dashed curve is the LL result. Parts a), b), and c) are for the Tevatron, LHC, and SSC center of mass energies, respectively.

5. Total cross section for $pp \to WZ + X$ as a function of the center of mass energy. Part a) is for $pp \to W^+Z + X$ and part b) is for $pp \to W^-Z + X$. The solid line is the NLL result, the long dashed line is the LL result, and the short dashed line is the LL calculation with the soft-gluon K-factor $K = 1 + \frac{4\pi}{9}\alpha_s$.

6. Decomposition of the total cross section for $pp \to W^{\pm}Z + X$ as a function of the center of mass energy. The NLL cross section (solid line) is decomposed into the LL contribution (long dashed line), the order α_s $q\bar{q}$ initial state contribution (dotted line), and the order α_s qg initial state contribution (short dashed line). Part a) is for $pp \to W^+Z + X$ and part b) is for $pp \to W^-Z + X$.

7. The order α_s finite virtual contribution to the NLL total cross section for $pp \to W^{\pm}Z + X$ as a function of the center of mass energy.

8. Invariant mass distribution of the WZ pair. The solid curve is the NLL result and the dashed curve is the LL result. Parts a) and b) are for the LHC and SSC center of mass energies, respectively.

9. Transverse momentum distribution of the Z-boson. The labeling conventions are the same as Fig. 8.

10. Rapidity distribution of the Z-boson. The labeling conventions are the same as Fig. 8.

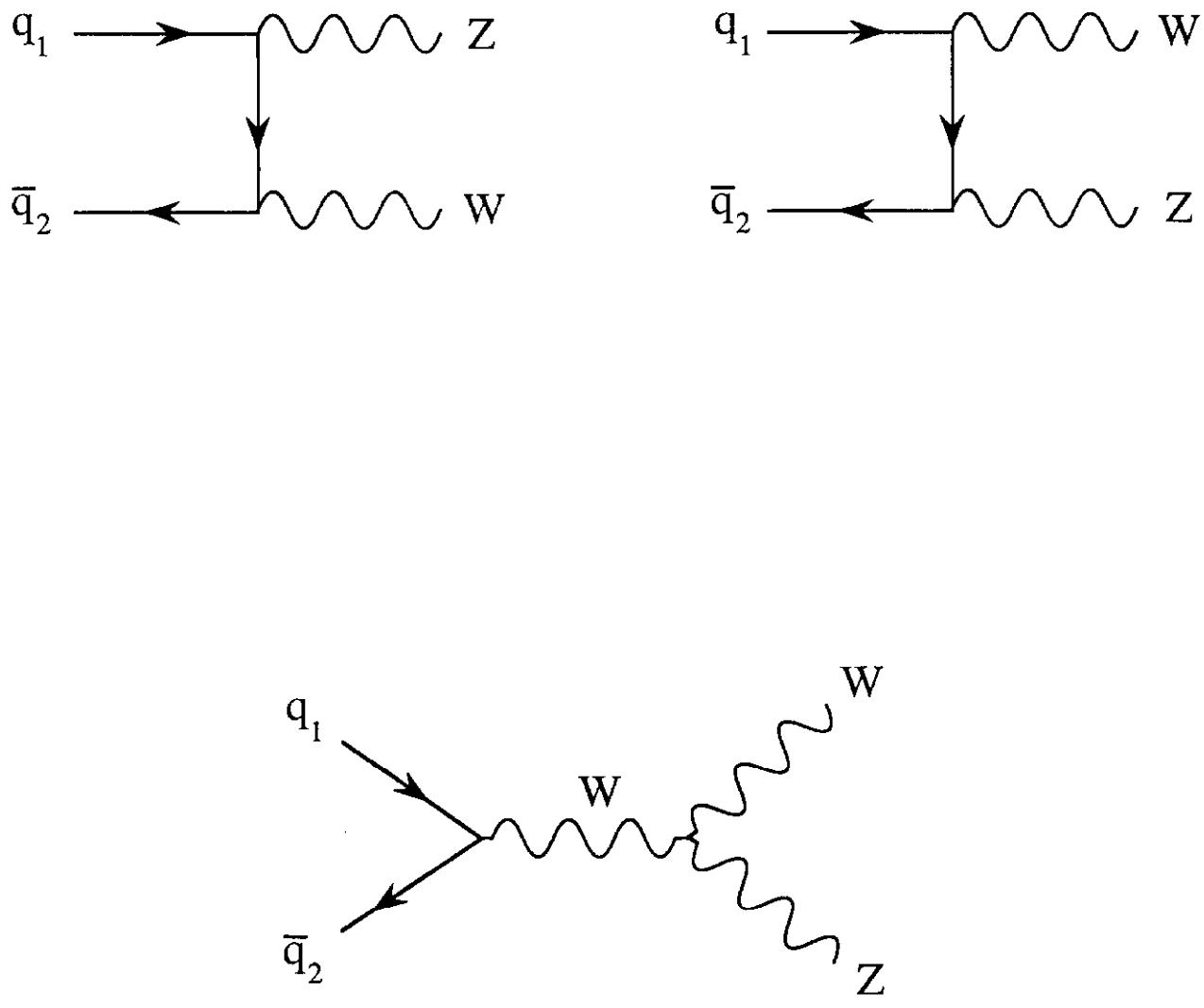

Fig. 1

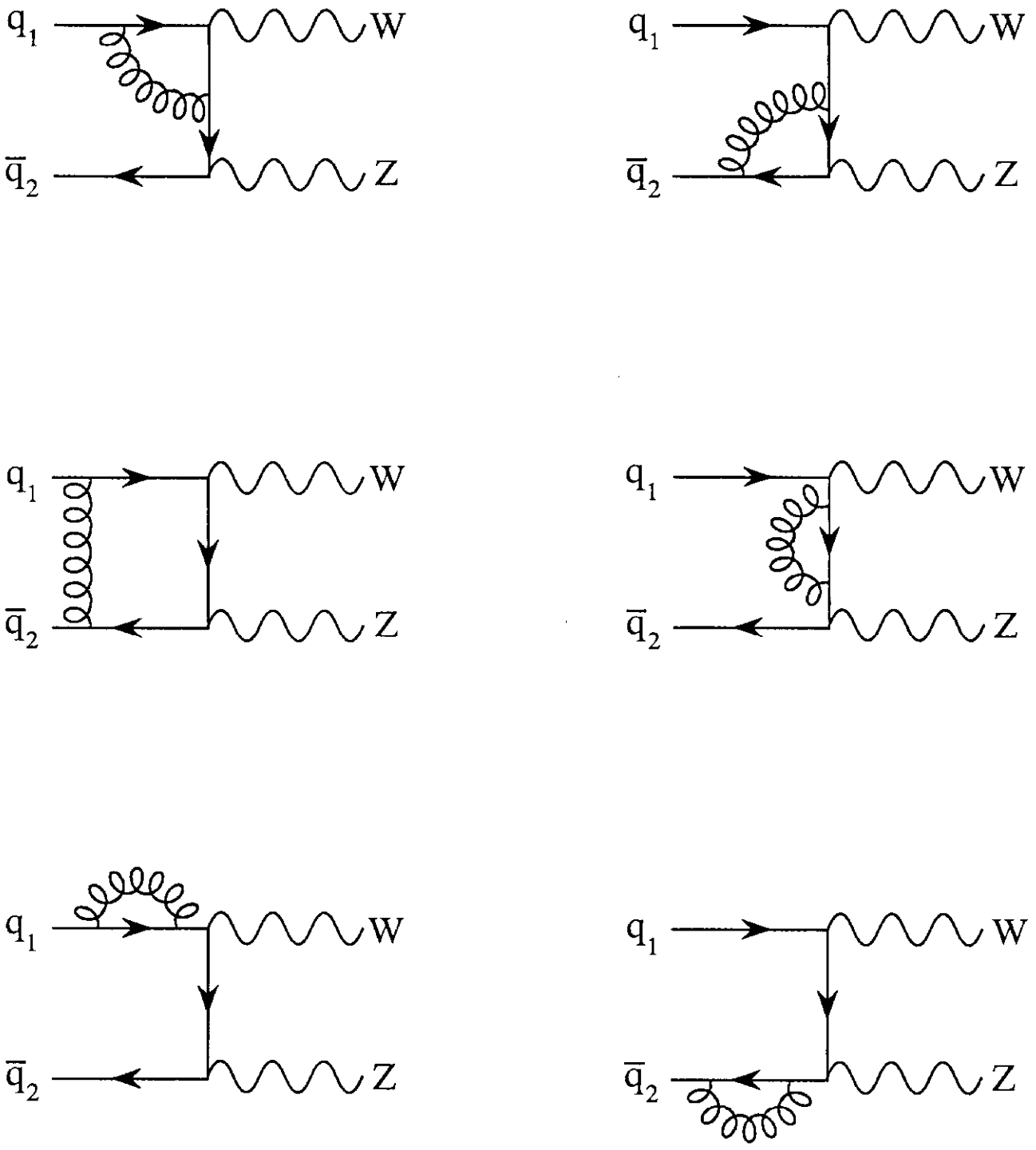

Fig. 2

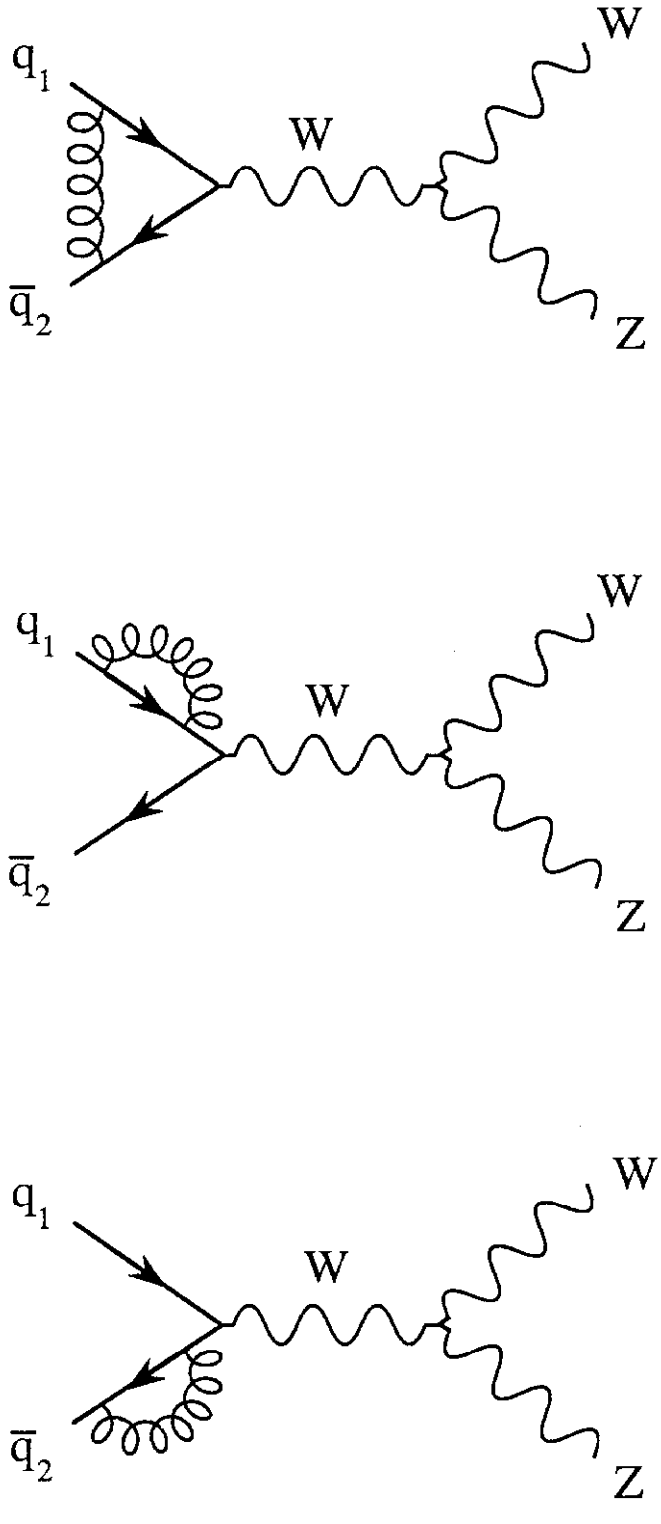

Fig. 2 (cont.)

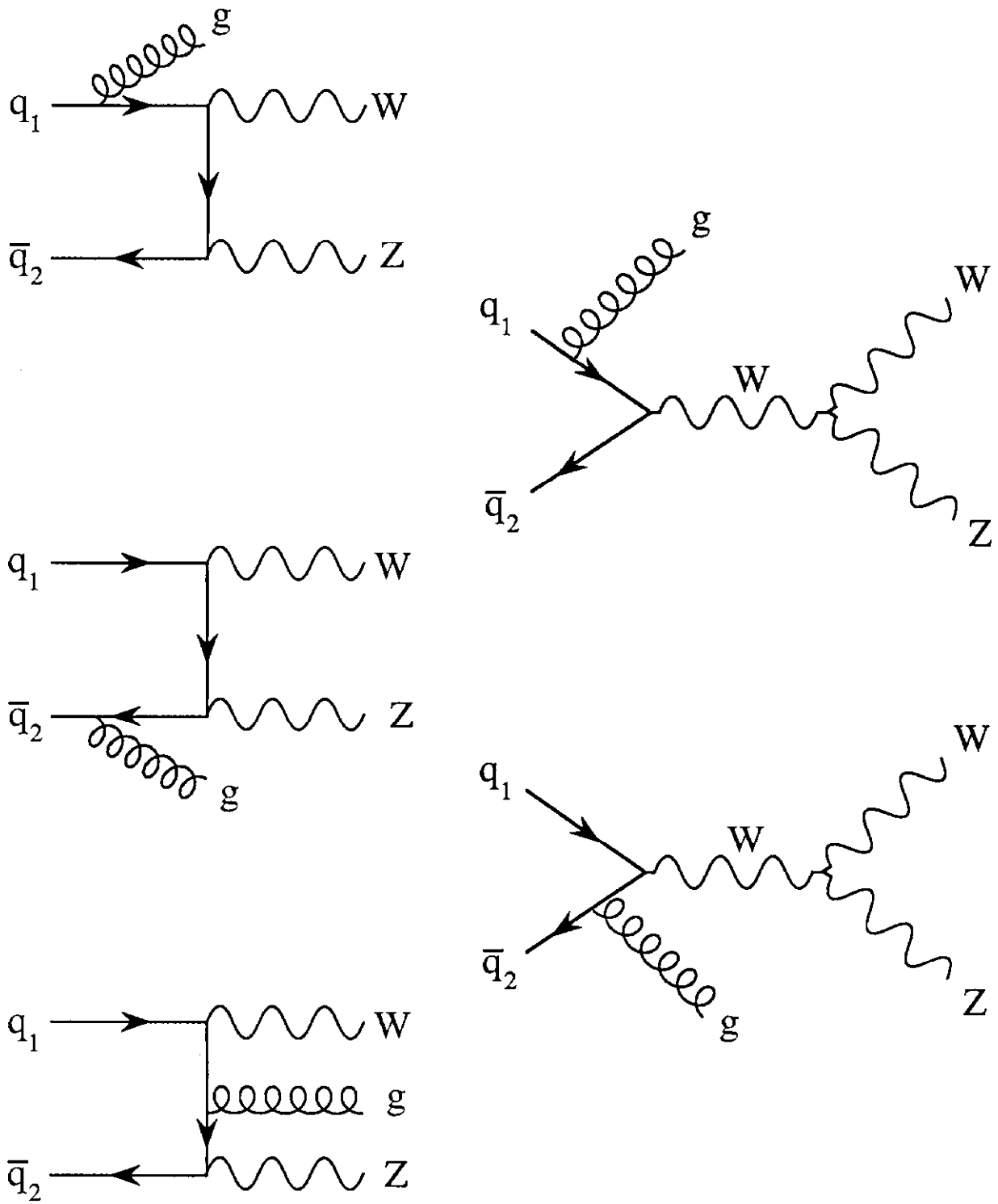

Fig. 3

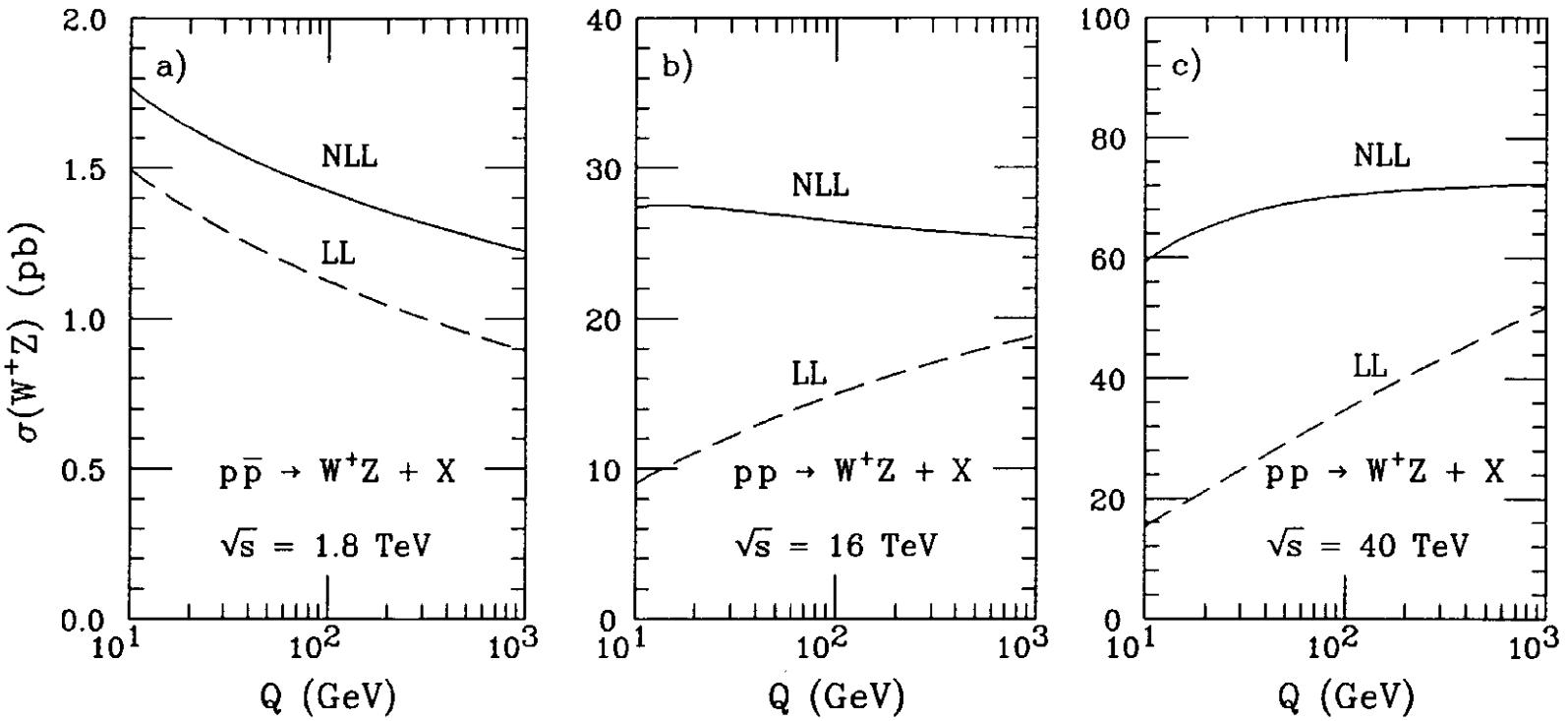
a)
NLL
LL
$p\bar{p} \rightarrow W^+Z + X$
$\sqrt{s}$ = 1.8 TeV
$\sigma(W^+Z)$ (pb)
Q (GeV)
b)
NLL
LL
$pp \rightarrow W^+Z + X$
$\sqrt{s}$ = 16 TeV
Q (GeV)
c)
NLL
LL
$pp \rightarrow W^+Z + X$
$\sqrt{s}$ = 40 TeV
Q (GeV)

Figure 4

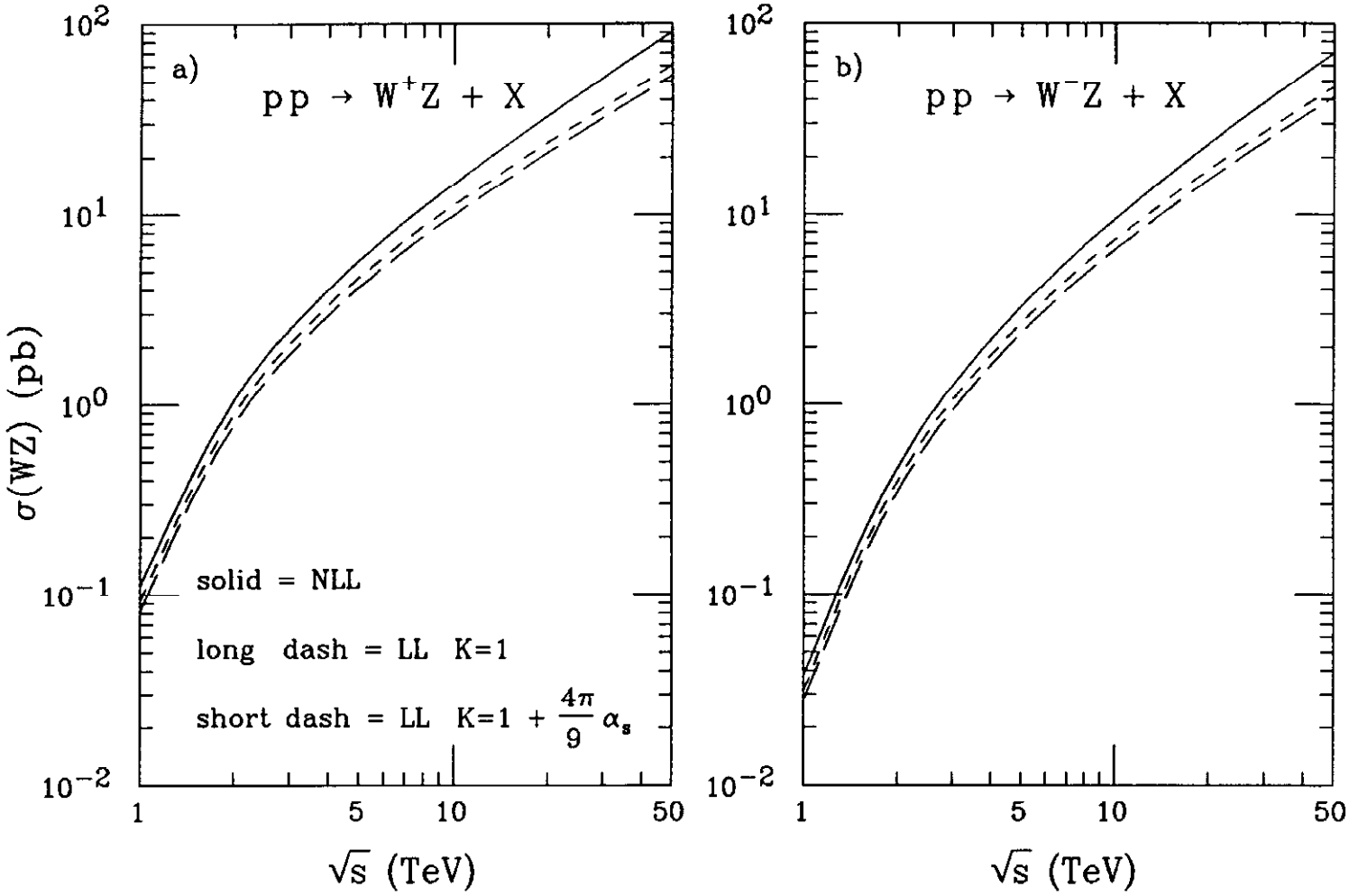
a)
pp → W⁺Z + X
b)
pp → W⁻Z + X
σ(WZ) (pb)
10²
10¹
10⁰
10⁻¹
10⁻²
1
5
10
50
√s (TeV)
solid = NLL
long dash = LL K=1
short dash = LL K=1 + 4π/9 α_s

Figure 5

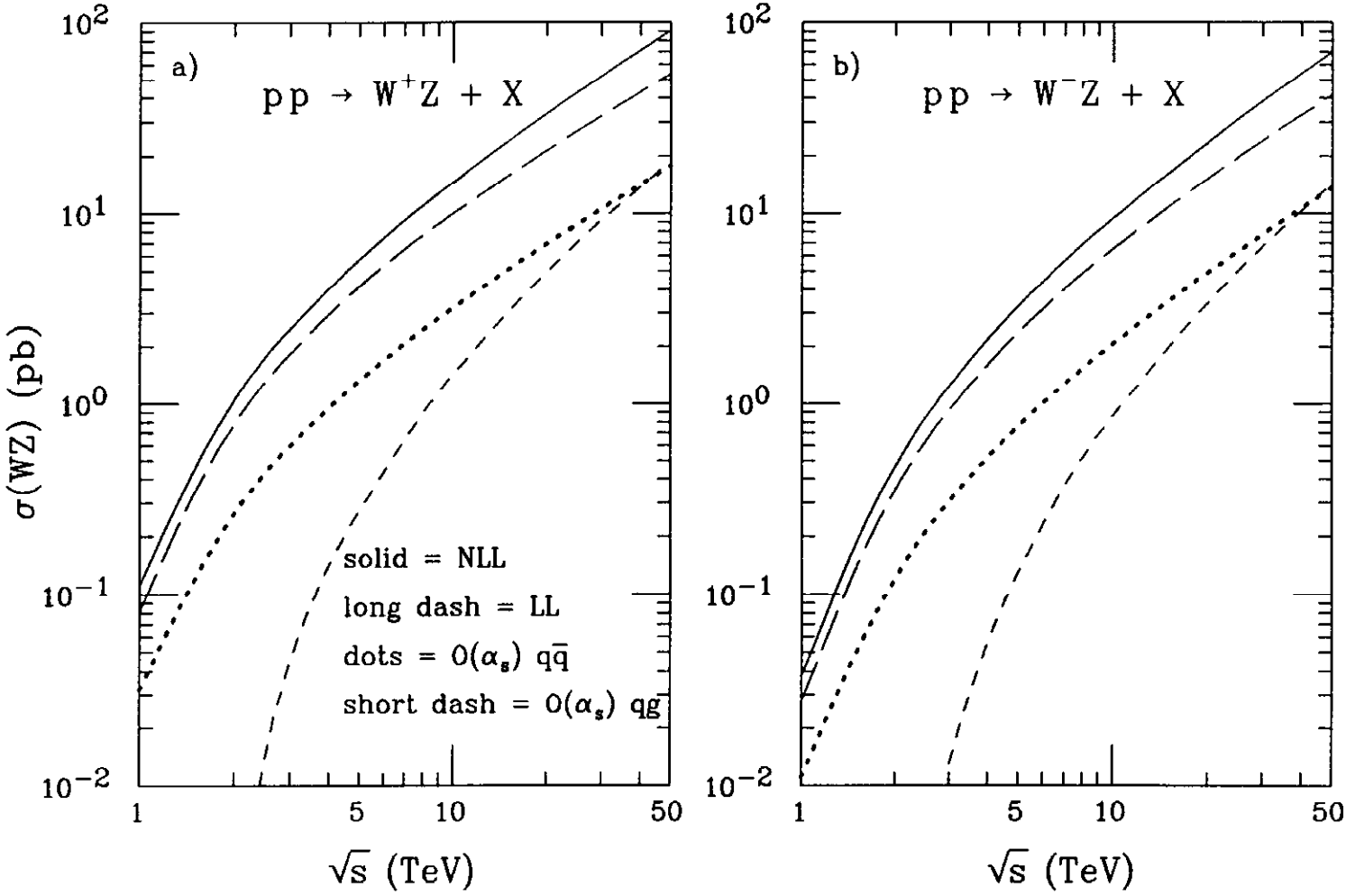
a)
pp → W⁺Z + X
b)
pp → W⁻Z + X
σ(WZ) (pb)
10²
10¹
10⁰
10⁻¹
10⁻²
1
5
10
50
√s (TeV)
solid = NLL
long dash = LL
dots = O(α_s) qq̄
short dash = O(α_s) qg

Figure 6

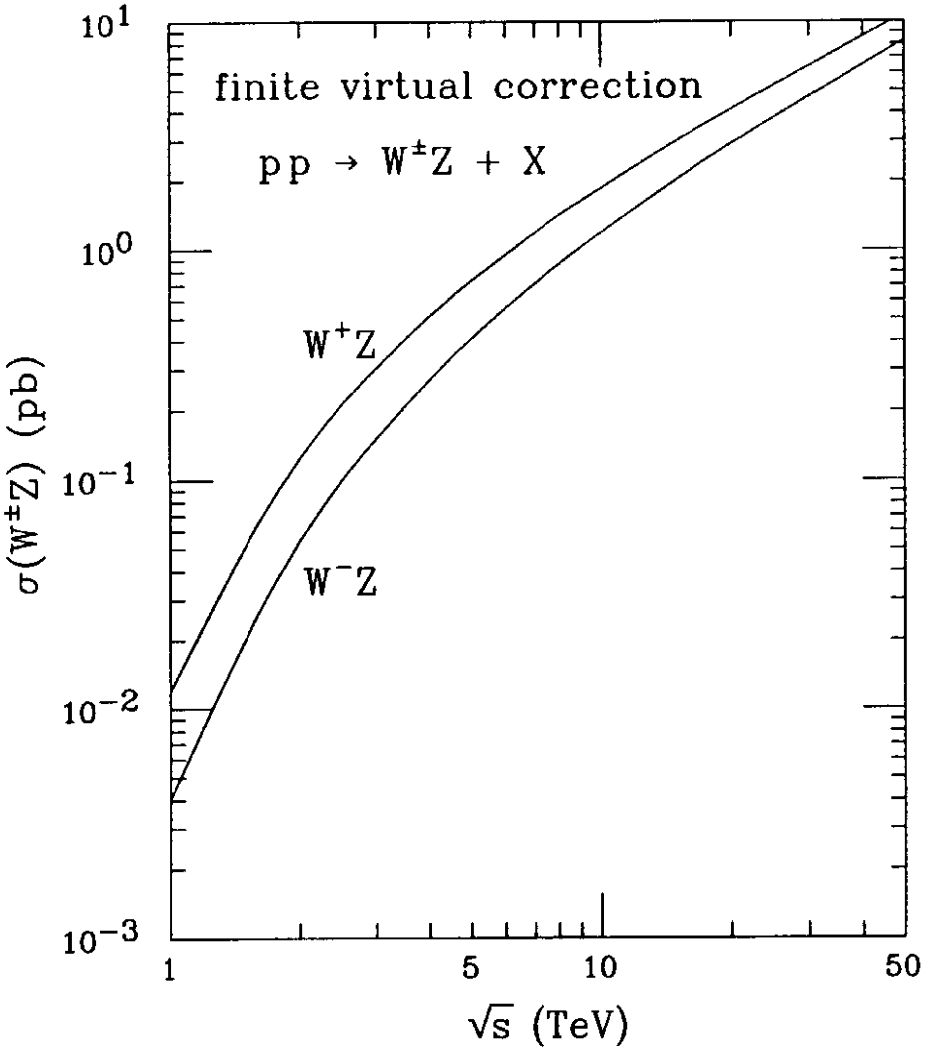
finite virtual correction
pp → W±Z + X
W+Z
W−Z
σ(W±Z) (pb)
√s (TeV)
10^1
10^0
10^−1
10^−2
10^−3
1
5
10
50

Figure 7

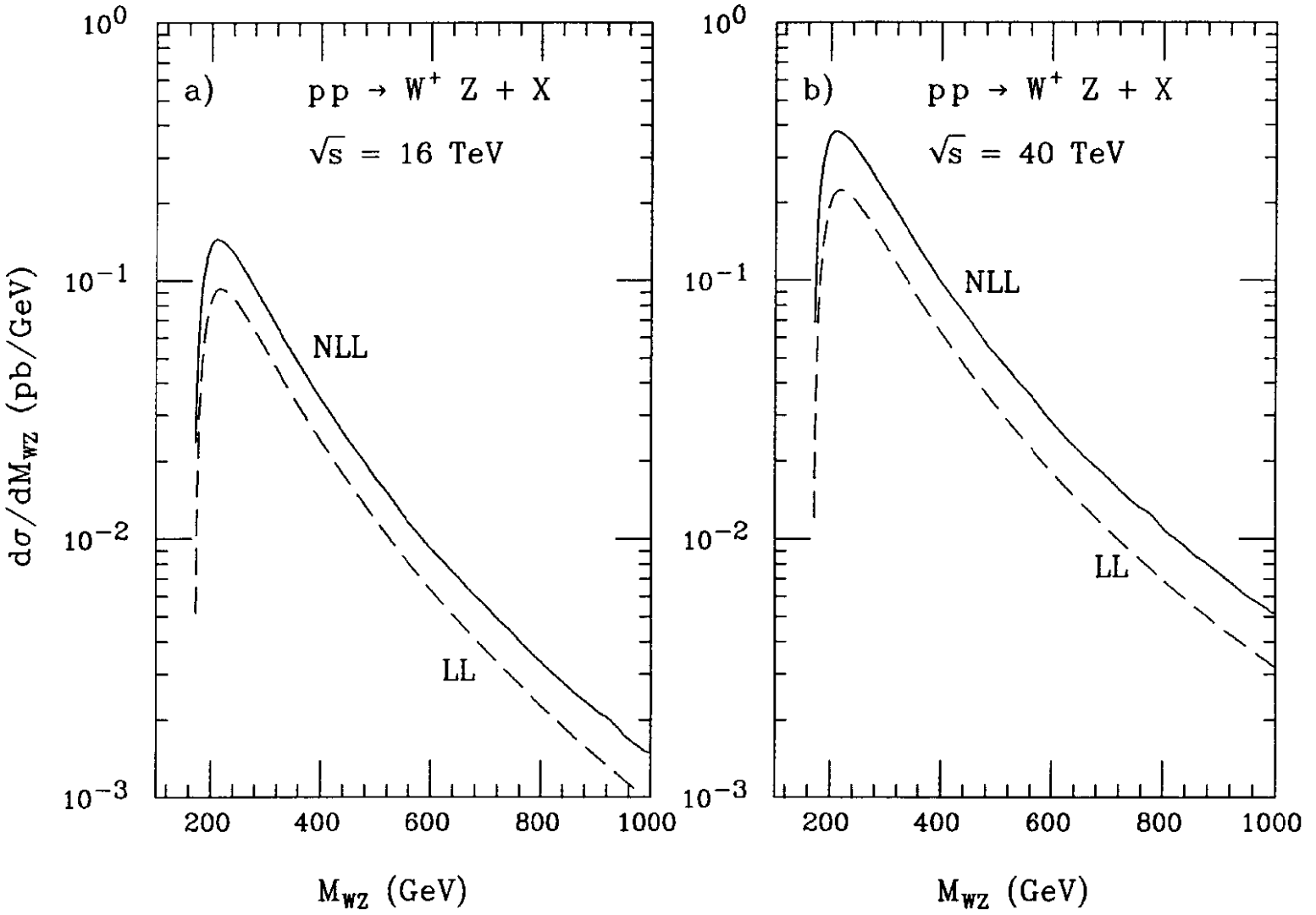
a)
pp → W+ Z + X
√s = 16 TeV
NLL
LL
b)
pp → W+ Z + X
√s = 40 TeV
NLL
LL
dσ/dMWZ (pb/GeV)
MWZ (GeV)
MWZ (GeV)
10^0
10^-1
10^-2
10^-3
200
400
600
800
1000

Figure 8

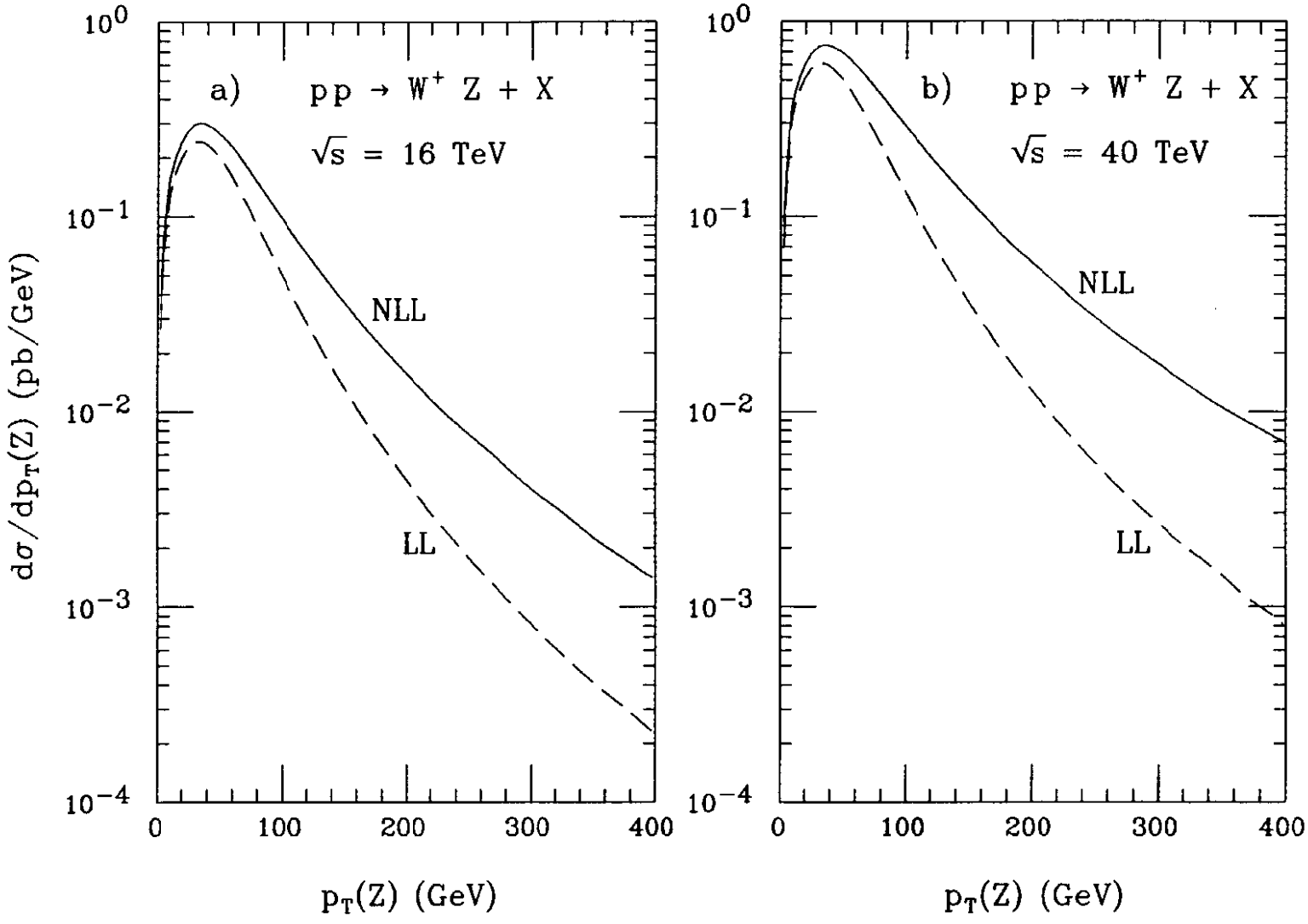
a)
pp → W+ Z + X
√s = 16 TeV
NLL
LL
dσ/dpT(Z) (pb/GeV)
pT(Z) (GeV)
b)
pp → W+ Z + X
√s = 40 TeV
NLL
LL
pT(Z) (GeV)

Figure 9

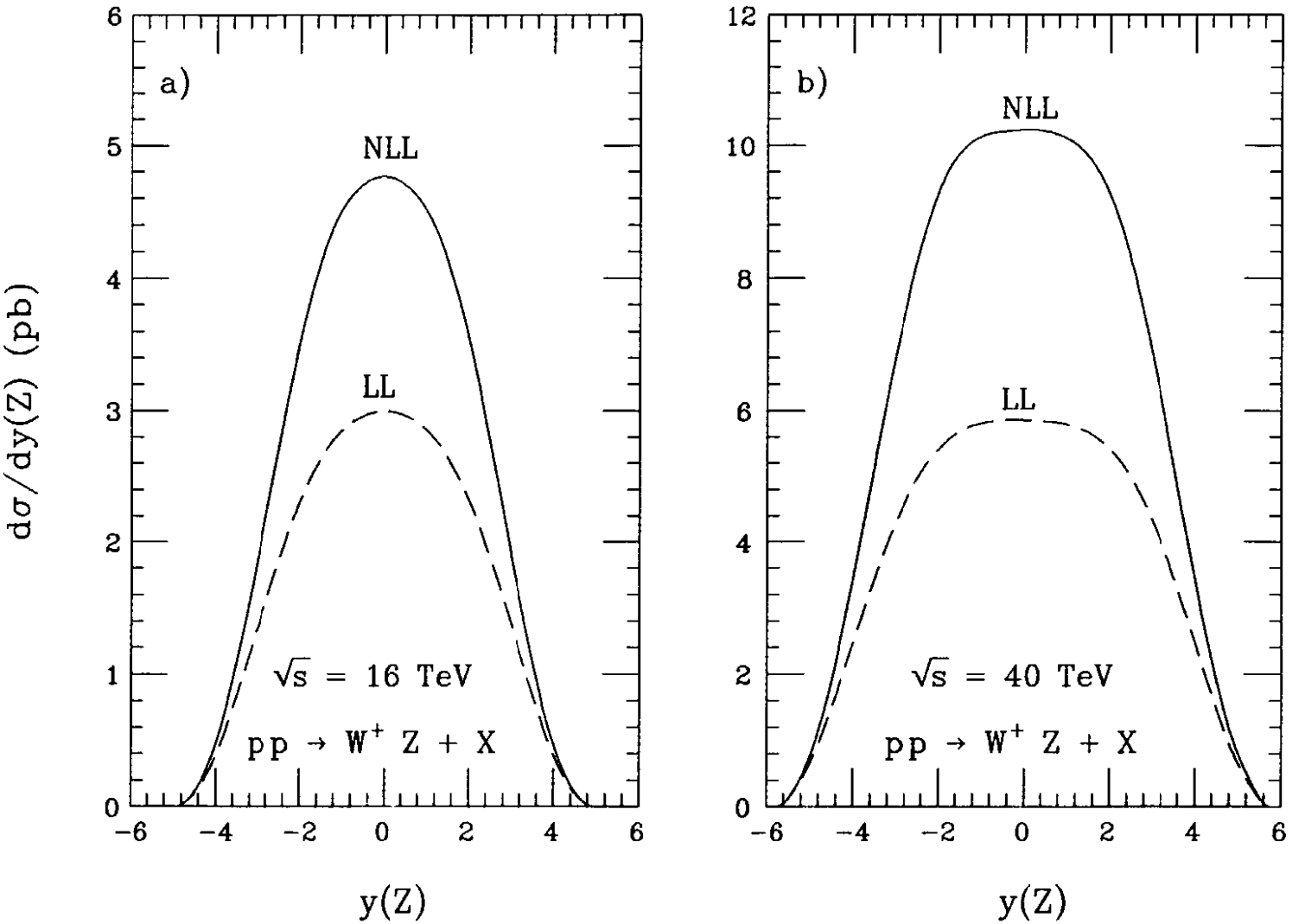

Figure 10